Available online at www.sciencedirect.com
ScienceDirect
Ceramics International 35 (2009) 693–698
CERAMICS INTERNATIONAL
www.elsevier.com/locate/ceramint

Preparation of titania-coated alumina film by electrolysis of $TiCl_4$-containing solution

Naoki Matsunaga [a], Yoshihiro Hirata [b,*], Yousuke Fukuda [a], Soichiro Sameshima [b]

[a] Department of Applied Chemistry and Chemical Engineering, Kagoshima University, 1-21-40 Korimoto, Kagoshima 890-0065, Japan
[b] Department of Advanced Nanostructured Materials Science and Technology, Kagoshima University, 1-21-40 Korimoto, Kagoshima 890-0065, Japan

Received 20 December 2007; received in revised form 8 January 2008; accepted 4 February 2008
Available online 5 June 2008

Abstract

Direct current in the range from 50 to 390 mA/cm^2 was flowed between alumina/tin-doped indium oxide (indium tin oxide, ITO) composite (cathode) and carbon (anode) electrodes in an aqueous solution containing $TiCl_4$ and $(NH_4)_2SO_4$ at pH 0.5. The composite electrode dissolved in the solution and was precipitated again on the surface of the electrode. The thickness of precipitated layer increased at a higher applied charge. During the electrolysis, TiO_2 was also deposited on the surface of precipitated layer. The amorphous TiO_2 heated at 300 °C and sintered Al_2O_3–ITO composite showed a good adsorption property of electromagnetic energy in the wide wavelength of 200–800 nm.

Keywords: B. Surfaces; C. Optical properties; D. Al_2O_3; TiO_2; Electrolysis

1. Introduction

Titanium oxide (TiO_2) is well known as an excellent photocatalyst in the ultraviolet wavelength range for the application of cosmetic, solar cell or coating material of window. Titania shows a phase transition from anatase (band gap, 3.2 eV) to rutile (band gap, 3.0 eV) at about 800 °C. Anatase has a higher catalytic activity than rutile. That is, a low temperature processing is needed to deposit strongly anatase on a substrate for many applications. Ohno et al. [1] reported that TiO_2 powder (rutile) has a high reflectivity of 90% (absorbance 10%) in the wavelength range of 420–750 nm but Ru-doped TiO_2 powder (rutile) decreases the reflectivity to 20–80%, depending on wavelength. Yui et al. [2] has confirmed that TiO_2 nanosheet electrodeposited on an indium tin oxide (ITO) electrode adsorbs the electromagnetic energy in the ultraviolet wave of 200–300 nm. Asahi et al. [3] reported that N-doped TiO_2 powder (anatase) improves the absorbance by 5–20% in the wavelength range of 400–500 nm. On the other hand, nanostructured TiO_2 thin films being composed of columnar-type grains [4,5], nanowires [6], nanorods [7], helical ribbon [8] and conical-shaped nanotubes [9,10] have been synthesized by plasma enhanced chemical vapor deposition, ion beam induced chemical vapor deposition [4], wet process [5], sol–gel electrophoresis deposition [6], reaction with hydrogen-bearing gas [7], anodic oxidation [8,10] and sol–gel polymerization [9]. Electrophoretic deposition (EPD) technique is also used for the fabrication of films of TiO_2 [11–15], Al_2O_3 [16,17] and CeO_2 [18] because of a short processing time, a simple apparatus and no shape restriction of substrate. Zhou et al. [11] prepared a TiO_2 film on F-doped SnO_2 (FTO)-coated glass using a TiO_2 aqueous suspension by EPD. The TiO_2 film with 480 nm thickness was composed of aggregated TiO_2 particles with sizes above 200 nm. Peralta-Hernández et al. [12] deposited TiO_2 and TiO_2–carbon composite film on ITO-coated glass. Above two papers [11,12] report a significant absorption of UV light shorter than 400 nm of wavelength in the deposited TiO_2 film. Yoon et al. [13] fabricated Au/TiO_2 or Pt/TiO_2 film on quartz glass or ITO glass substrate by co-sputtering method. Heat treatment of these films of 200–300 nm thickness at 600 °C improved the adsorption of the light at 650–700 nm of wavelength. Chu et al. [14,15] fabricated nanoporous TiO_2/Al_2O_3 composite films on ITO-coated glass by Al anodization and sol–gel process. The produced film showed a higher photocatalytic activity than a commercial TiO_2 powder. However, further effort is needed to use the electromagnetic energy of visible light.

* Corresponding author. Tel.: +81 99 285 8325; fax: +81 99 257 4742.
E-mail address: hirata@apc.kagoshima-u.ac.jp (Y. Hirata).

0272-8842/$34.00
doi:10.1016/j.ceramint.2008.02.012

Recently we found the phenomenon of dissolution-reprecipitation process of Al_2O_3–ITO (90 mass% In_2O_3–10 mass% SnO_2) system under the application of external voltage. This process forms a thick alumina layer on sintered dense Al_2O_3–ITO composite in an aqueous solution at room temperature. This paper reports the possibility of coprecipitation of TiO_2 precursor in alumina layer when the Al_2O_3–ITO composite was electrochemically treated in the solution containing a TiO_2 precursor. The reflectivity of the produced film in the wavelength of 200–800 nm was also measured.

2. Experimental procedure

A high purity α-Al_2O_3 powder of median size 150 nm (Al_2O_3 > 99.99 mass%, specific surface area 10.5 m^2/g, density 3.99 g/cm^3, Sumitomo Chemical Industry Co., Japan) and indium tin oxide powder of median size 200 nm (ITO, 90 mass% In_2O_3–10 mass% SnO_2, specific surface area 4.42 m^2/g, density 7.15 g/cm^3, Sumitomo Chemical Industry Co., Japan) were used as starting materials. As-received ITO powder was milled with 3 mol% Y_2O_3-stabilized ZrO_2 ball of 3 mm diameter for 24 h to break particle aggregate. Al_2O_3 and ITO powders were mixed at a volume ratio of 60–40 in an ethanol solution for 1 h. The dried mixed powder was uniaxially pressed at 60 MPa and then isostatically pressed at 200 MPa. The green compact was sintered at 1500 °C for 4 h in oxygen atmosphere (O_2: 99.7 vol%) to prevent the thermal decomposition of ITO. The bulk density measured by the Archimedes method with double-distilled water was 98.7% of theoretical density (5.25 g/cm^3). The sintered composite (diameter 10 mm, height 5 mm) and a cylindrical carbon (internal diameter 30 mm, external diameter 50 mm, height 40 mm) were used as working and counter electrodes, respectively. Ammonium sulfate ($(NH_4)_2SO_4$ > 99.5 mass%, mass%, Wako Pure Chemical Industries, Ltd., Japan) and titanium (IV) chloride solution (Ti: 16.0–17.0 mass%, Wako Pure Chemical Industries, Ltd., Japan) were dissolved in double-distilled water to control the $TiCl_4$ concentration (0–0.10 mol/l) and $(NH_4)_2SO_4$ concentration (0.2 mol/l) at pH 0.5. Fig. 1 shows the scheme of electrolysis apparatus [19–21]. The dense 60 vol% Al_2O_3–40 vol% ITO composite (working electrode) was set at the center of the cylindrical carbon electrode with Ag/AgCl reference electrode. The electrolysis was carried out in the current density range from 50 to 390 mA/cm^2 for 24 h. The corresponding electric field strength was 10 V/cm. After the electrolysis, the Al_2O_3–ITO electrode was dried at 100 °C for 24 h in air to observe the Al, In, Sn and Ti distribution by electron probe X-ray microanalyzer (EPMA, JXA-8600S/M, Japan Electron Optics Lab. Ltd., Japan) and the microstructure by scanning electron microscope (SM300, Topcon Technologies, Inc., Japan). Phase identification of the surface layers of Al_2O_3–ITO electrode heated at 700–900 °C were conducted using X-ray diffraction (RINT 2200PCH/KG, Rigaku Co., Japan). The photocatalysis property of the Al_2O_3–ITO electrode heated at 200–900 °C was measured by UV–vis spectrophotometer (UV-2450, Shimadzu Co., Japan).

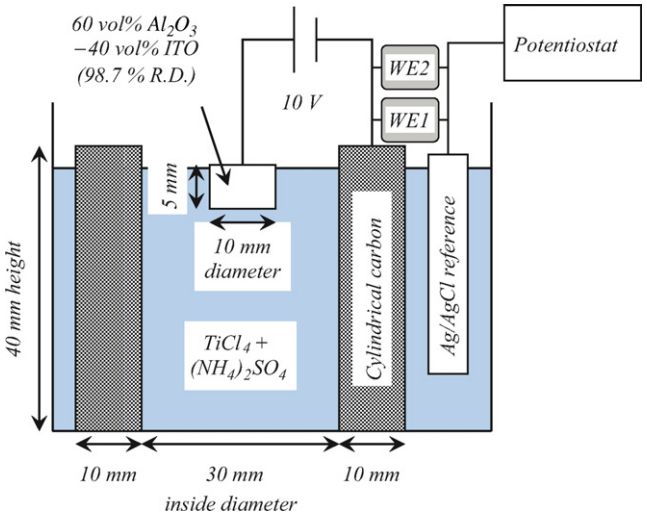

Fig. 1. Scheme of electrolysis apparatus.

3. Results and discussion

3.1. Current density of electrolysis

Fig. 2 shows time dependence of current density of the electrolysis at 10 V/cm of electric field strength. The electric potential of the Al_2O_3–ITO electrode and carbon electrode against Ag/AgCl reference electrode was 9.4–10.0 V and −0.6 to −0.2 V, respectively, in the solutions containing 0–0.10 M $TiCl_4$. No significant difference was measured in the electric potential with $TiCl_4$ concentration. The current density without $TiCl_4$ decreased slowly from 390 to 50 mA/cm^2 by 17 h of electrolysis time and increased at a longer electrolysis time. As discussed in latter section, Al_2O_3, In_2O_3 and SnO_2 components dissolved from the electrode, and these components were deposited again on the electrode surface. The decreased current density at the early stage is related to the formation of non-conductive alumina-rich layer. The increased current density after 17 h of electrolysis time may be due to the formation of conduction path through In_2O_3 or SnO_2 in the deposited layer. On the other hand, the current density in the solutions

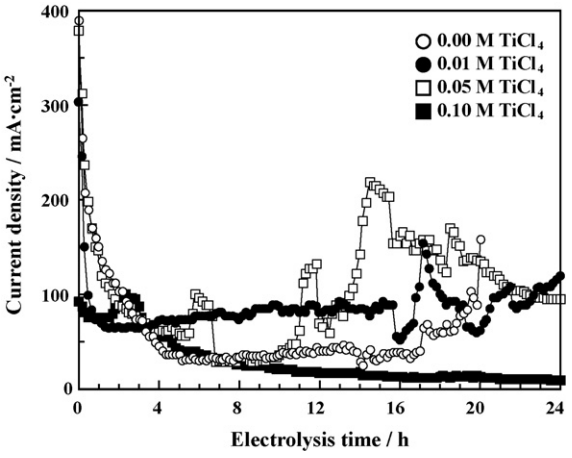

Fig. 2. Time dependence of current density at 10 V/cm of electric field strength.

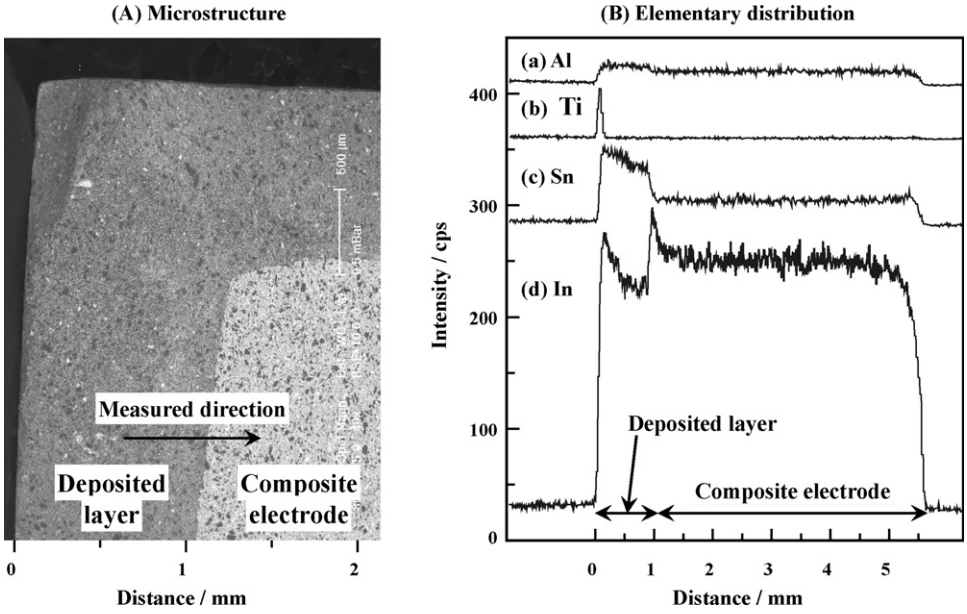

Fig. 3. Cross-section of Al_2O_3–ITO electrode (A) after the electrolysis in the solution containing 0.05 M $TiCl_4$ for 24 h and elementary distribution (B) of Al, In, Sn and Ti in the deposited layer.

containing $TiCl_4$ changed more up and down with time. This phenomenon reflects the competitive deposition of Al_2O_3, In_2O_3, SnO_2 and TiO_2. As explained latter, deposition of TiO_2 suppresses the electrolysis of H_2O.

3.2. Microstructure of deposited layer

Fig. 3 shows the cross-section of Al_2O_3–ITO electrode (A) and the elementary distribution (B) of Al, In, Sn and Ti in the deposited layer after the electrolysis in the solution containing 0.05 M $TiCl_4$ for 24 h. The deposited layer of 1.12 mm thickness contained Al, In and Sn components. The concentration of Al or In of deposited layer was comparable to that of Al or In of sintered Al_2O_3–ITO electrode. In the deposited layer a higher concentration of Sn was measured as compared with the inside concentration of the electrode. On the other hand, Ti component was rarely observed inside of the electrode. However, Ti component was highly measured on the surface of deposited layer. That is, Ti was not coprecipitated inside of the deposited layer. A similar deposition behavior of Al, In and Ti was observed in the other experimental results.

Fig. 4 shows the relation between electric charge of electrolysis for 24 h (area surrounded by the current density-time curve in Fig. 2) and (a) weight loss of the Al_2O_3–ITO electrode or (b) thickness of deposited layer. The dissolved amount of Al_2O_3–ITO composite increased at a higher electric charge during the electrolysis. The dissolved components were again deposited on the electrode. The increased concentration of $TiCl_4$ (0–0.05 M) enhanced the flowed electric charge but a too high concentration of $TiCl_4$ (0.10 M) suppressed the dissolution of the electrode, resulting in the decreased weight loss of the electrode and the decreased thickness of the deposited layer.

3.3. Electrochemical reaction

The $TiCl_4$ solution provided a low pH (~0.5) because of the hydrolysis of $TiCl_4$: $TiCl_4 + 2H_2O \rightarrow Ti(OH)_2^{2+} + 2H^+ + 4Cl^-$. The electrolysis of acidic solution produces H_2 and O_2 gas at anode (carbon electrode) and cathode (Al_2O_3–ITO electrode) by Eqs. (1) and (2), respectively:

$$2H^+ + 2e^- \rightarrow H_2, \quad E^\circ = 0\,V \tag{1}$$

$$2H^+ + \tfrac{1}{2}O_2 + 2e^- \rightarrow H_2O, \quad E^\circ = 1.23\,V \tag{2}$$

where E° represents standard electrode potential. The total electrolysis reaction corresponds to Eq. (3) (Eqs. (1) and (2)).

$$H_2O \rightarrow H_2 + \tfrac{1}{2}O_2, \quad E^\circ(3) = E^\circ(1) - E^\circ(2) = -1.23\,V \tag{3}$$

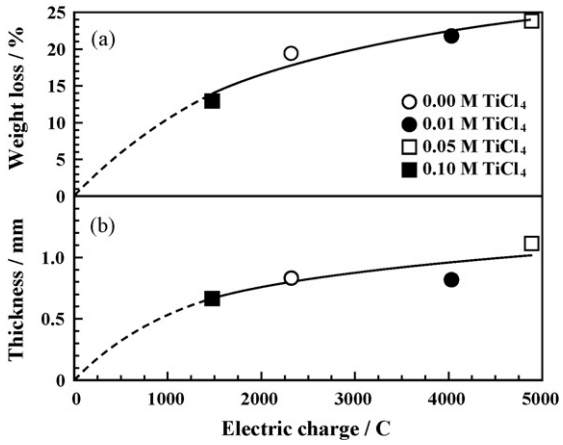

Fig. 4. Weight loss of the Al_2O_3–ITO electrode (a) and thickness of deposited layer (b) after the electrolysis for 24 h.

The Gibbs free energy (ΔG°) for Eq. (3) is related to $E^\circ(3)$ by the following equation:

$$\Delta G^\circ(3) = -nFE^\circ(3) \quad (4)$$

where $n(2)$ is the number of electrons transferred from cathode to anode and F the Faraday constant. Since $E^\circ(3)$ is a negative value, $\Delta G^\circ(3)$ results in a positive value. That is, an external applied voltage above 1.23 V is needed to proceed the reaction by Eq. (3). The weight loss of Al_2O_3–ITO electrode and the thickness of the deposited layer are closely related to the electrolysis of the solution (Fig. 4). According to the phase diagrams of Al_2O_3–H_2O, In_2O_3–H_2O and SnO_2–H_2O systems [22], the following ions dissolve from the corresponding hydroxide or oxide at a low pH to reach a solubility limit.

$$Al_2O_3 + 3H_2O \rightarrow 2Al(OH)_3 \rightarrow 2Al^{3+} + 6OH^-, \quad E^\circ = -0.66\,V \quad (5)$$

$$In_2O_3 + 3H_2O \rightarrow 2In(OH)_3 \rightarrow 2In^{3+} + 6OH^-, \quad E^\circ = -0.70\,V \quad (6)$$

$$SnO_2 + 2H_2O \rightarrow Sn^{4+} + 4OH^-, \quad E^\circ = -0.94\,V \quad (7)$$

The above reaction is coupled with the cathode reaction (Eq. (2)) to explain the result in Fig. 4. A possible reaction of Al_2O_3 component in cathode is proposed by Eqs. (8) and (9).

$$H_2O \rightarrow 2H^+ + \tfrac{1}{2}O_2 + 2e^-, \quad E^\circ = -1.23\,V \quad (8)$$

$$2H^+ + Al_2O_3 + 3H_2O \rightarrow Al(OH)_3 + 2H_2O + Al^{3+} + OH^-, \quad E^\circ = -0.20\,V \quad (9)$$

The total reaction at cathode is expressed by the following equation.

$$Al_2O_3 + 2H_2O \rightarrow \tfrac{1}{2}O_2 + 2e^- + Al(OH)_3 + Al^{3+} + OH^-, \quad E^\circ = -1.43\,V \quad (10)$$

Eq. (10) explains both the increased weight loss and the increased thickness of the deposited layer. A similar reaction for In_2O_3 and SnO_2 components are presented by Eqs. (11) and (12), respectively:

$$In_2O_3 + 2H_2O \rightarrow \tfrac{1}{2}O_2 + 2e^- + In(OH)_3 + In^{3+} + OH^- \quad (11)$$

$$SnO_2 + H_2O \rightarrow \tfrac{1}{2}O_2 + 2e^- + Sn^{4+} + 2OH^-, \quad E^\circ = -3.51\,V \quad (12)$$

Eq. (12) suggests that no deposition of Sn component occurs during the electrolysis of the solution. However, Sn component was observed in the deposited layer (Fig. 3). This result suggests the formation of $Sn(OH)_4$ from Sn^{4+} and OH^- ions produced in Eq. (12). That is, a part of SnO_2 dissolved is again deposited as $Sn(OH)_4$.

On the other hand, the relation between $Ti(OH)_2^{2+}$ ions formed from $TiCl_4$ and electrolysis of solution (Eq. (8)) is proposed by the following equation.

$$Ti(OH)_2^{2+} + \tfrac{1}{2}O_2 + 2e^- + H_2O \rightarrow Ti(OH)_4 \quad (13)$$

Total reaction is presented by the following equation:

$$Ti(OH)_2^{2+} + 2H_2O \rightarrow Ti(OH)_4 + 2H^+, \quad E^\circ = 0.77\,V \quad (14)$$

The Gibbs free energy for Eq. (14) is a negative value because of the positive value of E° (0.77 V), suggesting a high possibility of the coupled reaction (Eqs. (8) and (13)) at the cathode. That is, the electrons and O_2 gas produced at the cathode are consumed by $Ti(OH)_2^{2+}$ ions. This reaction causes the decrease of amount of electrons transferred to anode and leads to the decreased current density. The above reaction explains the decreased current density of the solution containing 0.10 mol/l $TiCl_4$ in Fig. 2.

3.4. Heated Al_2O_3–ITO electrode

Fig. 5 shows the X-ray diffraction patterns for the surface of Al_2O_3–ITO electrode heated at 700–900 °C in air. Alpha-Al_2O_3, In_2O_3 solid solution (ITO) and SnO_2 were recognized in the starting powder and heated electrode. Rutile was also included in the electrode heated at 800–900 °C. In addition, unknown phase was observed in the electrodes heated at 700–900 °C. The result in Fig. 5 suggests that $Ti(OH)_4$ deposited on the surface of the electrode changed to amorphous phase below 700 °C and crystallized to rutile at a higher temperature.

Fig. 6 shows UV–vis spectra of the Al_2O_3–ITO electrode after the electrolysis with 0.05 M $TiCl_4$ for 24 h and subsequently heated at 200–900 °C. The electrodes heated above 400 °C showed the increase of reflectance at around 380 nm (band gap 3.3 eV), because TiO_2 formed adsorbed the energy of electromagnetic wave of shorter wavelength. The heating at a low temperature of 200–300 °C was most effective to absorb the energy in the wide wavelength (200–800 nm). The formed $Ti(OH)_4$ changes to amorphous phase or anatase of low crystallinity at 300 °C. The crystallization to rutile lost the absorption of the electromagnetic energy at 400–800 nm of wavelength.

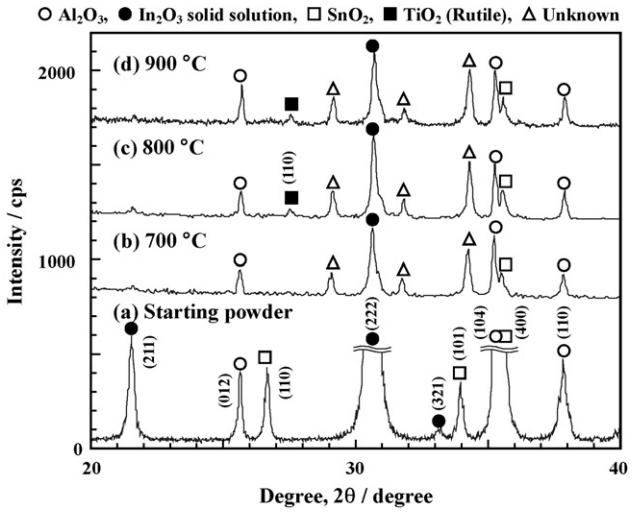

Fig. 5. X-ray diffraction patterns of the starting powder and Al_2O_3–ITO electrode after heating at 700–900 °C.

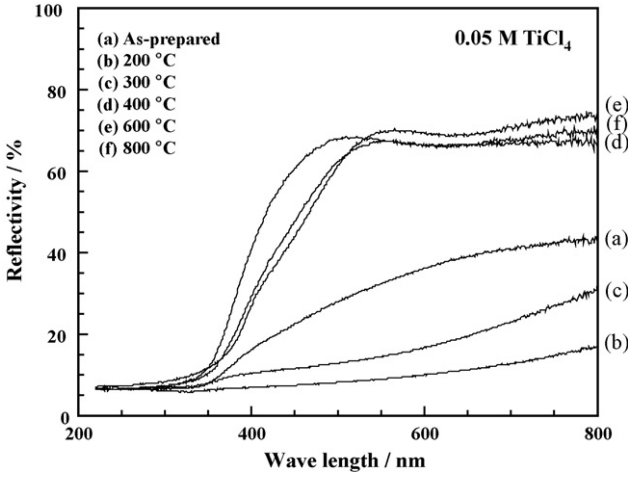

Fig. 6. UV–vis spectra of the Al_2O_3–ITO electrode after the electrolysis with 0.05 mol/l $TiCl_4$ and subsequently heated at 200–900 °C.

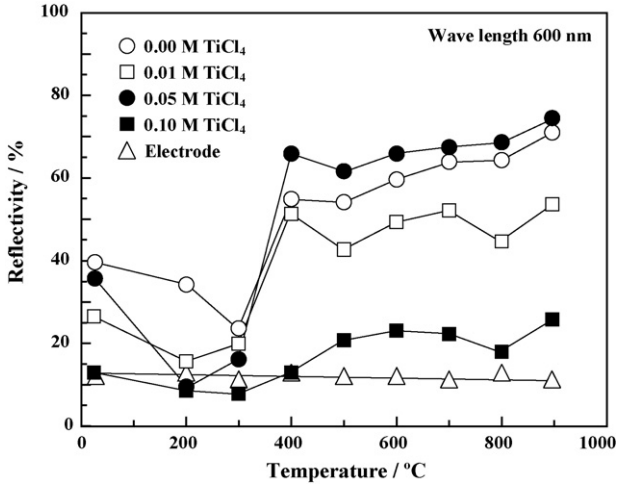

Fig. 8. Reflectively of Al_2O_3–ITO–TiO_2 film and sintered Al_2O_3–ITO composite at 600 nm of wavelength as a function of calcination temperature.

Fig. 7 shows UV–vis spectra of (a) Al_2O_3 powder, (b) ITO powder, (c) 60 vol% Al_2O_3–40 vol% ITO mixed powder and (d) sintered Al_2O_3–ITO composite. The reflectivity of Al_2O_3 powder was almost 100% in the wide wavelength of 200–800 nm. On the other hand, the reflectivity of ITO powder was small in the wavelength range shorter than 350 nm and increased in the longer wavelength range. The reflectivity of Al_2O_3–ITO mixed powder was similar to that of ITO powder because of the high reflectivity of Al_2O_3 powder. However, the Al_2O_3–ITO composite sintered at 1500 °C adsorbed the electromagnetic wave in the wide wavelength of 200–800 nm. This phenomenon is very interesting and studied in future.

Fig. 8 shows the reflectively at 600 nm of Al_2O_3–ITO–TiO_2 film as a function of calcination temperature. The reflectively of the Al_2O_3–ITO–TiO_2 film was very low below 300 °C and increased above 400 °C. Interesting result is a low reflectivity of Al_2O_3–ITO–TiO_2 film prepared by the electrolysis with 0.10 M $TiCl_4$ and the sintered Al_2O_3–ITO electrode in the wide wavelength of 200–800 nm. This result indicates the small effect of crystallinity of TiO_2 on the adsorption of electromagnetic wave. The structure of TiO_2 at atomic scale will be observed in a next paper.

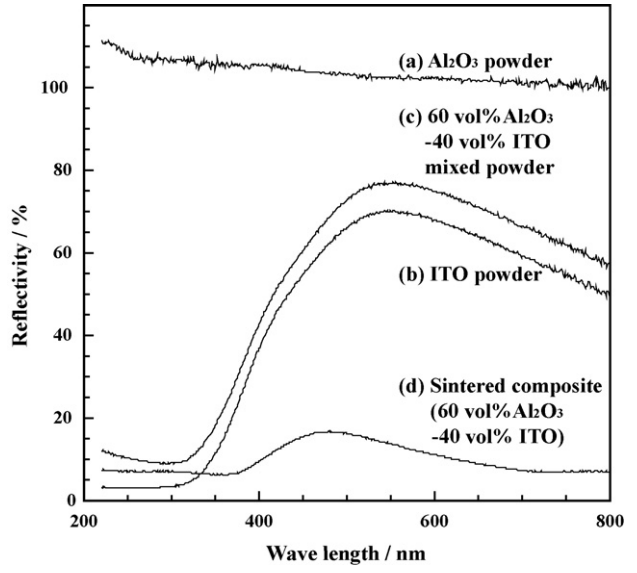

Fig. 7. UV–vis spectra of (a) Al_2O_3 powder, (b) ITO powder, (c) 60 vol% Al_2O_3–40 vol% ITO mixed powder and (d) sintered Al_2O_3–ITO composite.

4. Conclusions

Electrolysis of aqueous solutions containing $TiCl_4$ of 0–0.1 mol/l was carried out at 10 V/cm of electric filed strength between dense Al_2O_3 (60 vol%)–ITO (40 vol%) cathode and carbon anode.

(1) The current density decreased at the early stage of electrolysis and changed up and down at a longer time.
(2) The amount of Al_2O_3 and ITO dissolved from the electrode increased at a higher electric charge during the electrolysis. The dissolved components were again deposited on the electrode.
(3) Ti component was not included inside of the deposited layer and observed on only the surface of deposited layer.
(4) The electrochemical deposition of Al and In components is interpreted by the cathode reaction of M_2O_3 (M = Al, In) + $2H_2O \rightarrow 1/2O_2 + 2e^- + M(OH)_3 + M^{3+} + OH^-$. SnO_2 dissolves electrochemically as follows: $SnO_2 + H_2O \rightarrow 1/2O_2 + 2e^- + Sn^{4+} + 2OH^-$. A part of the dissolved Sn^{4+} and OH^- ions were deposited again as $Sn(OH)_4$. $Ti(OH)_2^{2+}$ ions produced from $TiCl_4$ react with O_2 gas and electrons produced at the cathode ($H_2O \rightarrow 2H^+ + 1/2O_2 + 2e^-$) to form $Ti(OH)_4$ ($Ti(OH)_2^{2+} + 1/2O_2 + 2e^- + H_2O \rightarrow Ti(OH)_4$). This reaction reduced the current density during the electrolysis in the $TiCl_4$-rich solution because of the consumption of electrons formed.
(5) The deposited $Ti(OH)_4$ changed to amorphous phase below 700 °C and crystallized to rutile above 800 °C. The amorphous TiO_2 heated at 300 °C was most effective to

absorb the electromagnetic energy in the wide wavelength (200–800 nm). The reflectivity of Al_2O_3–ITO electrode was also very low in the wide wavelength of 200–800 nm.

References

[1] T. Ohno, F. Tanigawa, K. Fujihara, S. Izumi, M. Matsumura, Photocatalytic oxidation of water by visible light using ruthenium-doped titanium dioxide powder, J. Photochem. Photobiol. A: Chem. 127 (1999) 107–110.

[2] T. Yui, Y. Mori, T. Tsuchino, T. Itoh, T. Hattori, Y. Fukushima, K. Takagi, Synthesis of photofunctional titania nanosheets by electrophoretic deposition, Chem. Mater. 17 (2005) 206–211.

[3] R. Asahi, T. Morikawa, T. Ohwaki, K. Aoki, Y. Taga, Visible-light photocatalysis in nitrogen-doped titanium oxides, Science 293 (2001) 269–271.

[4] F. Gracia, J.P. Holgado, A.R. González-Elipe, Photoefficiency and optical microstructural, and structural properties of TiO_2 thin film used as photoanodes, Langmuir 20 (2004) 1688–1697.

[5] T. Kudo, Y. Nakamura, A. Ruike, Development of rectangular column structured titanium oxide photocatalysts anchored on silica sheets by a wet process, Res. Chem. Intermed. 29 (2003) 631–639.

[6] Y. Lin, G.S. Wu, X.Y. Yuan, T. Xie, L.D. Zhang, Fabrication and optical properties of TiO_2 nanowire arrays made by sol–gel electrophoresis deposition into anodic alumina membranes, J. Phys.: Condens. Matter 15 (2003) 2917–2922.

[7] S. Yoo, S.A. Akbar, K.H. Sandhage, Nanocarving of bulk titania crystals into oriented arrays of single-crystal nanofibers via reaction with hydrogen-bearing gas, Adv. Mater. 16 (2004) 260–264.

[8] D. Gong, C.A. Grimes, O.K. Varghese, W. Hu, R.S. Singh, Z. Chen, E.C. Dickey, Titanium oxide nanotube arrays prepared by anodic oxidation, J. Mater. Res. 16 (2001) 3331–3334.

[9] J.H. Jung, H. Kobayashi, K.J.C. van Bommel, S. Shinkai, T. Shimizu, Creation of novel helical ribbon and double-layered nanotube TiO_2 structures using an organogel template, Chem. Mater. 14 (2002) 1445–1447.

[10] G.K. Mor, O.K. Varghese, M. Paulose, N. Mukherjee, C.A. Grimes, Fabrication of tapered, conical-shaped titania nanotubes, J. Mater. Res. 18 (2003) 2588–2593.

[11] M. Zhou, J. Yu, S. Liu, P. Zhai, L. Jiang, Effects of calcination temperatures on photocatalytic activity of SnO_2/TiO_2 composite films prepared by an EPD method, J. Hazard. Mater. 154 (2008) 1141–1148.

[12] J.M. Peralta-Hernández, J. Manríquez, Y. Meas-Vong, F.J. Rodríguez, T.W. Chapman, M.I. Maldonado, L.A. Godínez, Photocatalytic properties of nano-structured TiO_2-carbon films obtained by means of electrophoretic deposition, J. Hazard. Mater. 147 (2007) 588–593.

[13] J.W. Yoon, T. Sasaki, N. Koshizaki, Dispersion of nanosized noble metals in TiO_2 matrix and their photoelectrode properties, Thin Solid Films 483 (2005) 276–282.

[14] S.Z. Chu, K. Wada, S. Inoue, S. Todoroki, Synthesis and characterization of titania nanostructures on glass by Al anodization and sol–gel process, Chem. Mater. 14 (2002) 266–272.

[15] S.Z. Chu, S. Inoue, K. Wada, D. Li, J. Suzuki, Fabrication and photocatalytic characterizations of ordered nanoporous X-doped (X = N, C, S, Ru, Te, and Si) TiO_2/Al_2O_3 films on ITO/glass, Langmuir 21 (2005) 8035–8041.

[16] B. Ferrari, R. Moreno, Electrophoretic deposition of aqueous alumina slip, J. Eur. Ceram. Soc. 17 (1997) 549–556.

[17] Y. Hirata, A. Nishimoto, Y. Ishihara, Forming of alumina powder by electrophoretic deposition, J. Ceram. Soc. Jpn. 99 (1991) 108–113.

[18] K. Kamada, K. Higashikawa, M. Inada, N. Enomoto, J. Hojo, Photo-assisted anodic electrodeposition of ceria thin films, J. Phys. Chem. C 111 (2007) 14508–14513.

[19] Y. Hirata, H. Hatano, H. Kyoda, K. Hamasaki, Synthesis of alumina/nickel composite by electrodeposition of nickel, J. Mater. Res. 10 (1995) 2697–2699.

[20] Y. Hirata, H. Kyoda, T. Iwamoto, K. Hamasaki, Electro deposition of nickel into porous alumina compact, J. Ceram. Soc. Jpn. 103 (1995) 460–463.

[21] Y. Hirata, H. Kyoda, T. Iwamoto, H. Hatano, K. Hamasaki, Infiltration of nickel into alumina compact by electrodeposition, Ceram. Trans. 51 (1995) 237–241.

[22] C.F. Baes Jr., R.E. Mesmer, The Hydrolysis of Cations, Krieger Publishing Company, Malabar, FL, 1986, p. 122, 150, 322 and 356.